THE COMPANY OF
Biologists

RESEARCH ARTICLE

High-resolution imaging of cardiomyocyte behavior reveals two distinct steps in ventricular trabeculation

David W. Staudt[1,2], Jiandong Liu[1,3], Kurt S. Thorn[1], Nico Stuurman[4], Michael Liebling[5] and Didier Y. R. Stainier[1,2,6,7,*]

ABSTRACT

Over the course of development, the vertebrate heart undergoes a series of complex morphogenetic processes that transforms it from a simple myocardial epithelium to the complex 3D structure required for its function. One of these processes leads to the formation of trabeculae to optimize the internal structure of the ventricle for efficient conduction and contraction. Despite the important role of trabeculae in the development and physiology of the heart, little is known about their mechanism of formation. Using 3D time-lapse imaging of beating zebrafish hearts, we observed that the initiation of cardiac trabeculation can be divided into two processes. Before any myocardial cell bodies have entered the trabecular layer, cardiomyocytes extend protrusions that invade luminally along neighboring cell-cell junctions. These protrusions can interact within the trabecular layer to form new cell-cell contacts. Subsequently, cardiomyocytes constrict their abluminal surface, moving their cell bodies into the trabecular layer while elaborating more protrusions. We also examined the formation of these protrusions in trabeculation-deficient animals, including *erbb2* mutants, *tnnt2a* morphants, which lack cardiac contractions and flow, and *myh6* morphants, which lack atrial contraction and exhibit reduced flow. We found that, compared with cardiomyocytes in wild-type hearts, those in *erbb2* mutants were less likely to form protrusions, those in *tnnt2a* morphants formed less stable protrusions, and those in *myh6* morphants extended fewer protrusions per cell. Thus, through detailed 4D imaging of beating hearts, we have identified novel cellular behaviors underlying cardiac trabeculation.

KEY WORDS: Cardiac cell biology, Morphogenesis, Trabeculation, *erbb2*, Live imaging, Zebrafish

INTRODUCTION

The adult heart is composed of a number of substructures optimized for pumping blood. In order to create this efficient pump, the heart undergoes complex morphogenetic changes during development, all while continuing to beat and maintain blood flow to the developing animal. One early morphogenetic process is the development of the ventricular trabeculae. Ventricular trabeculae are ridge-like myocardial structures within the walls of the ventricles that form a complex network early in development (Sedmera et al., 2000; Stankunas et al., 2008; Liu et al., 2010; Peshkovsky et al., 2011; Staudt and Stainier, 2012). Trabeculae are crucial for heart function, as mutations that abrogate trabecular formation are embryonic lethal (Gassmann et al., 1995; Lee et al., 1995; Meyer and Birchmeier, 1995; Suri et al., 1996; Morris et al., 1999; Tidcombe et al., 2003; Liu et al., 2010), and human patients with hypertrabeculation exhibit a form of heart failure (Jenni et al., 1999). The trabeculae serve to increase myocardial mass before the formation of coronary vessels and, as such, have been shown to contribute to ventricular contractility; they are also necessary for the formation of the conduction system (Sedmera et al., 2003; Liu et al., 2010). Although studies in mouse have started to reveal the genetic basis of cardiac trabeculation, how cardiomyocytes form these important structures while continuously contracting remains relatively unknown. Most challenging for these *in vivo* studies is the fact that the heart is constantly moving, and so obtaining high-resolution images over time required novel image-processing techniques. Zebrafish are amenable to long-term imaging of the developing heart (Beis and Stainier, 2006), thereby providing an ideal model system in which to study cardiac trabeculation with cellular resolution in real time.

A number of factors are known to play a role in trabeculation. Several signaling pathways, including the Angiopoietin/Tie2 (Suri et al., 1996), Semaphorin/Plexin (Toyofuku et al., 2004a; Toyofuku et al., 2004b) and the Neuregulin/ErbB2/ErbB4 (Gassmann et al., 1995; Lee et al., 1995; Morris et al., 1999; Tidcombe et al., 2003; Liu et al., 2010) pathways have been implicated in the process. Among these regulators of trabeculation, the ErbB2 pathway has been implicated to be important cell-autonomously in cardiomyocytes (Morris et al., 1999; Tidcombe et al., 2003; Liu et al., 2010). Additionally, mechanical factors such as blood flow and/or cardiac contractility contribute to trabeculation. Zebrafish larvae with severe defects in cardiac contractility due to disrupted sarcomeres fail to form trabeculae (Chi et al., 2008). Disrupting blood flow through the ventricle by disrupting atrial contractility leads to impaired trabeculation (Peshkovsky et al., 2011). Similarly, disrupting flow into the left ventricle of embryonic chick hearts by left atrial ligation decreases left ventricular trabecular volume (Sedmera et al., 1999). It is currently unknown how ErbB2 signaling or mechanical forces regulate trabeculation.

Most of what we know about trabeculation comes from end point analyses of mutants, which can reveal whether or not embryos develop trabeculae. However, no studies have addressed how cardiomyocytes form trabeculae at the cellular level. Previous studies have reported the location of cardiomyocytes in the trabecular layer starting at 55 hours postfertilization (hpf) in zebrafish (Chi et al., 2008; Liu et al., 2010; Peshkovsky et al., 2011).

[1]Department of Biochemistry and Biophysics, University of California, San Francisco, CA 94158, USA. [2]Cardiovascular Research Institute, University of California, San Francisco, CA 94158, USA. [3]Department of Pathology and Laboratory Medicine and McAllister Heart Institute, University of North Carolina at Chapel Hill, Chapel Hill, NC 27599, USA. [4]The Howard Hughes Medical Institute and the Department of Cellular and Molecular Pharmacology, University of California, San Francisco, CA 94158, USA. [5]Electrical and Computer Engineering Department, University of California, Santa Barbara, CA 93106, USA. [6]Program in Developmental and Stem Cell Biology, University of California, San Francisco, CA 94158, USA. [7]Department of Developmental Genetics, Max Planck Institute for Heart and Lung Research, Ludwigstr. 43, 61231 Bad Nauheim, Germany.

*Author for correspondence (didier.stainier@mpi-bn.mpg.de)

Development

Additionally, although studies in mouse and chick indicate that trabecular cardiomyocytes are clonally related to cardiomyocytes in the outer, compact layer (Mikawa et al., 1992; Meilhac et al., 2003; Meilhac et al., 2004a; Meilhac et al., 2004b), our recent cell lineage-tracing data (Liu et al., 2010), as well as data from Gupta and Poss (Gupta and Poss, 2012), indicate that trabeculation occurs via a process of delamination, rather than asymmetric cell division. How cardiomyocytes delaminate from the compact layer remains unclear. Here, using a combination of clonal analysis and live cell imaging of beating hearts, we show that trabeculae are formed by a two-step delamination process. Cardiomyocytes first extend luminal protrusions over their neighbors, and then gradually constrict their abluminal surface to move their cell body into the trabecular layer. Further, we find that mutations that disrupt trabeculation cause distinct defects in the formation and behavior of these myocardial protrusions. In hearts that do not contract, cardiomyocytes extend short-lived protrusions, whereas in hearts with reduced blood flow, cardiomyocytes extend fewer protrusions per cell. Finally, in *erbb2* mutants, fewer cardiomyocytes extend protrusions. Thus, we identify a differentially regulated cellular process that contributes to the first steps of trabeculation.

RESULTS

Cardiomyocytes extend long protrusions before the first trabeculae appear

Although many mutant studies have reported trabeculation defects, the dynamics of the process remain unclear. In order to study the cellular behaviors underlying the emergence of trabeculae, we employed a combination of high-speed spinning disk confocal microscopy and post-acquisition temporal alignment to acquire 3D time-lapse movies of beating hearts (Liebling et al., 2005; Ohn et al., 2009) (Fig. 1A-D; supplementary material Movie 1). In brief,
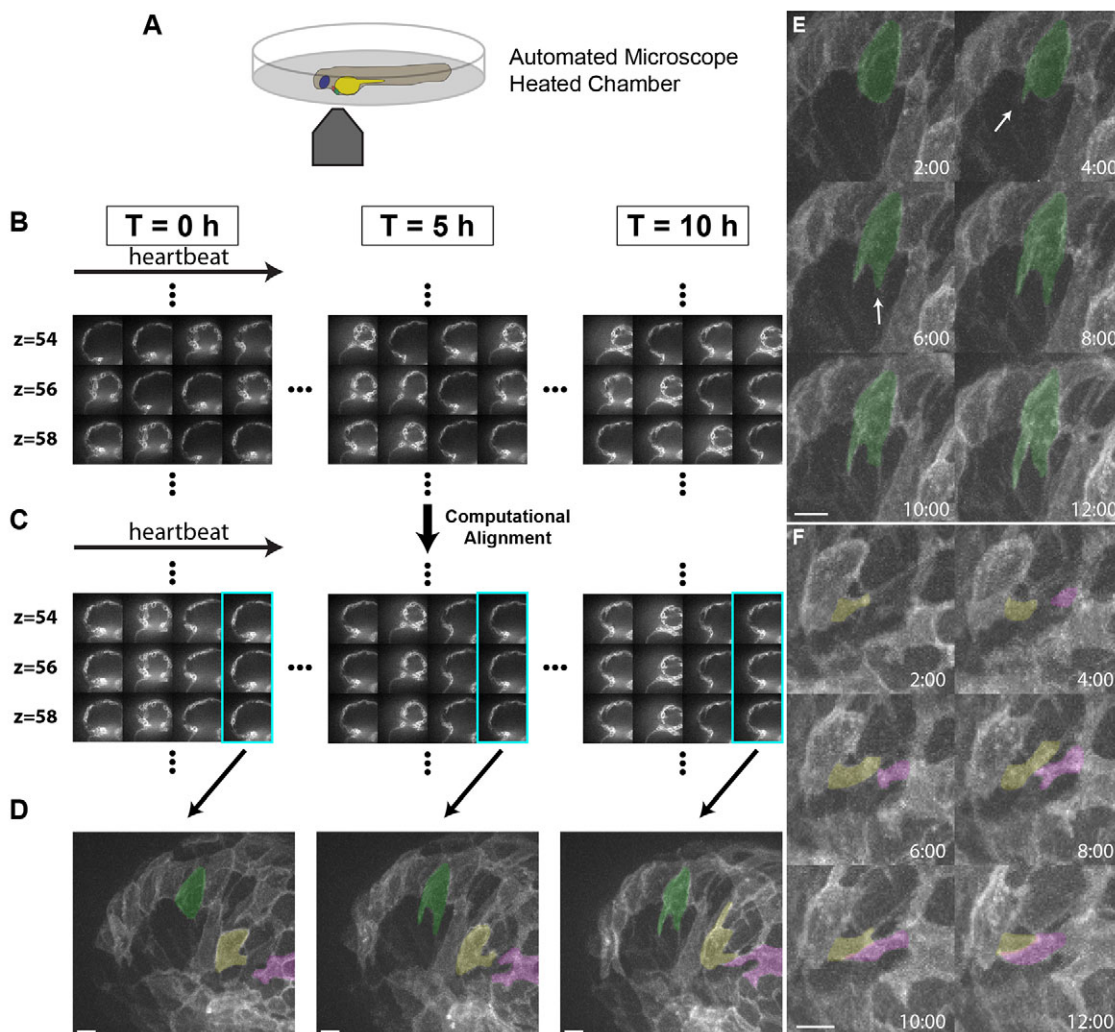
Fig. 1. Live imaging reveals the dynamics of cardiomyocyte protrusions. (A) Zebrafish embryos at 55-60 hpf were imaged in glass plates on an automated, inverted microscope equipped with a spinning disk. (B-D) Steps in the data processing pipeline. The three columns show datasets acquired from the same embryo at the indicated time points after the start of imaging. (B) Data are initially acquired as unsynchronized z-stacks of movies. Frames from three sequential z-slices are shown. Note that the rows (z-slices) are unsynchronized. (C) Frames following computational alignment: sequences from each z-slice are temporally registered (e.g. delayed or advanced) to match those in other z-slices and developmental stages. The turquoise box contains the frame during ventricular relaxation that is used for further analysis. (D) Maximum intensity z-projections of the relaxed ventricle from the three developmental time points. Individual cardiomyocytes are pseudocolored green, magenta and yellow. Note the dramatic cell shape changes that can be observed after computational alignment. (E) Time-lapse images of cellular protrusions. A cardiomyocyte extending protrusions is marked in green. Arrows point to the emerging protrusions. (F) Time-lapse images of two protrusions, highlighted in yellow and purple, extending towards each other. The two protrusions appear to form a cell-cell junction by 12 hours of imaging. Scale bars: 10 μm.

we used a spinning disk microscope run by a custom script to obtain confocal movies of beating zebrafish hearts at sequential *z*-levels. The script allowed for repeated imaging of multiple positions corrected for *z*-drift. *z*-stacks of movies were obtained at multiple developmental time points between 55 and 76 hpf. These movies were triggered without regard to the stage of the cardiac contraction cycle, and so were unsynchronized (Fig. 1B). Using previously published image-alignment algorithms (Liebling et al., 2005; Liebling et al., 2006; Ohn et al., 2009), these stacks of movies were synchronized post-acquisition, yielding 3D movies of hearts at regularly spaced intervals within the cardiac cycle, allowing us to focus on the heart at ventricular diastole, when the ventricle is most expanded (Fig. 1C,D). We could then examine cellular behaviors over the course of development without the complicating motion of normal contraction. Strikingly, live imaging of *Tg(myl7:ras-GFP)* embryos revealed that a large proportion of cardiomyocytes extend long protrusions along the surface of the heart (supplementary material Movie 2). Live imaging of mosaically marked ventricular cardiomyocytes revealed that ~48% extended protrusions (Fig. 5D; *n*=103 cardiomyocytes from 16 embryos). These protrusions extended slowly, taking 8-10 hours to reach their full length of 10-20 μm (Fig. 1E; supplementary material Movie 3). Occasionally, protrusions from different cardiomyocytes extended towards one another, made contact, and stayed connected for many hours (Fig. 1F; supplementary material Movie 4). Using mosaic analysis, we observed such cell-cell contacts in five pairs of cardiomyocytes out of 103 imaged.

In order to examine these protrusions more closely, we generated embryos mosaically expressing a random combination of fluorescent proteins in the cytoplasm of *Tg(myl7:ras-GFP)* cardiomyocytes by Tol2-mediated transgenesis (Kawakami, 2007). Plasmids were generated in which the myocardial *myl7* promoter drives expression of either the red TagRFP-T (Shaner et al., 2008), blue TagBFP (Subach et al., 2008) or near-infrared IRFP (Filonov et al., 2011). Co-injection of these three plasmids generated numerous, multi-colored cardiomyocytes that could be uniquely tracked. The cytoplasmic fluorescent proteins allowed us to unambiguously identify cardiomyocytes throughout the 3D structure of the heart, while the membrane GFP allowed us to relate marked cardiomyocytes to their unmarked neighbors, as well as to the overall structure of the myocardium. This approach allowed us to identify these invading membrane-bound structures as protrusions

from cardiomyocytes that remained in contact with the abluminal surface of the myocardial epithelium (Fig. 2A-B′). Interestingly, these protrusions tended to extend above cell-cell junctions of neighboring cardiomyocytes (Fig. 2B). To determine whether these protrusions persisted within the trabeculae, we used the same technique and examined hearts at 78 hpf, which is ~24 hours after trabeculation has begun. Cardiomyocytes with long protrusions were readily visible within the trabecular layer (Fig. 2C,C′). Thus, cardiomyocytes begin to extend protrusions before a trabecular layer is present, and trabecular cardiomyocytes can possess similarly long protrusions.
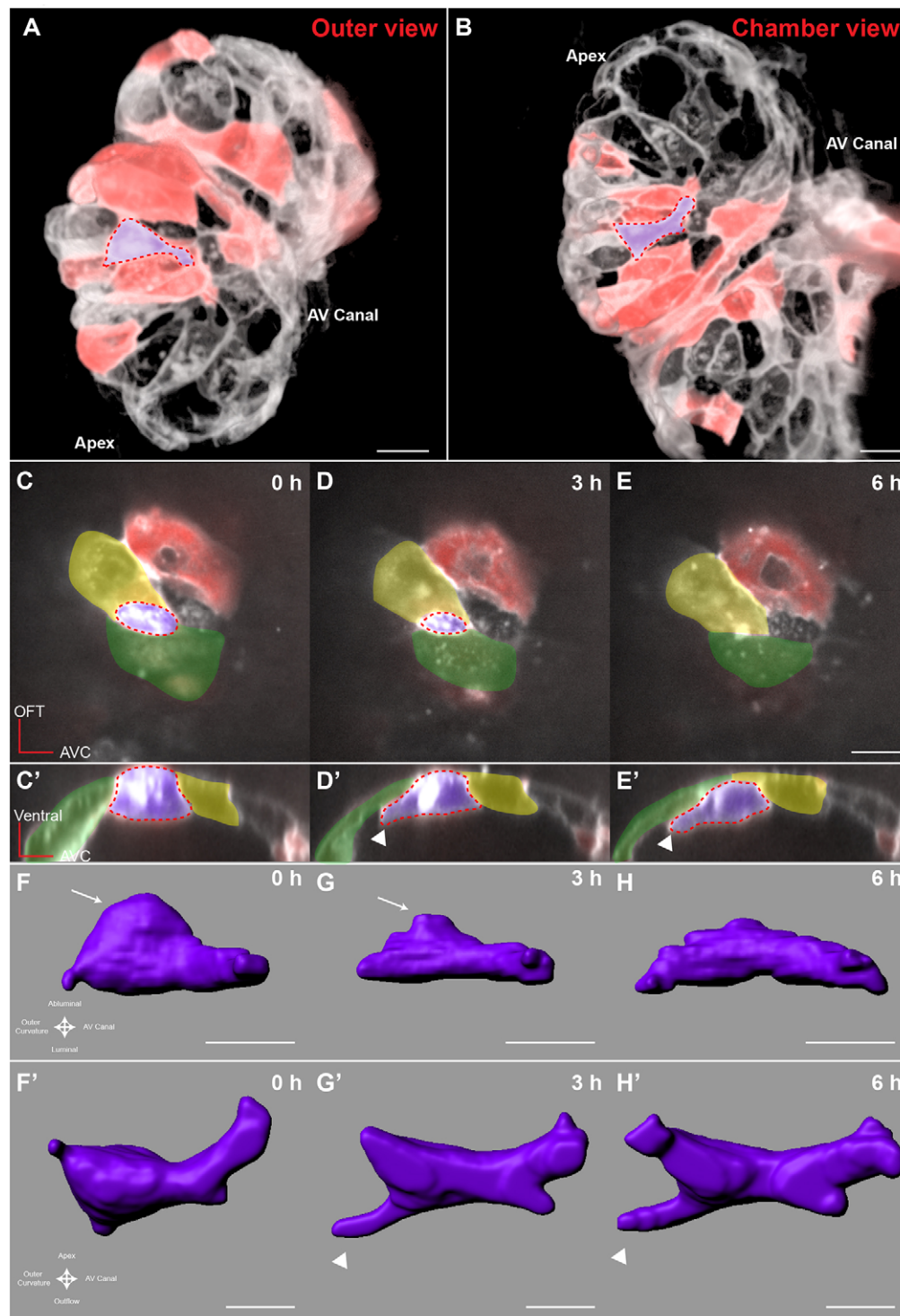
Cardiomyocytes constrict their abluminal surface while extending protrusions to enter the trabecular layer

Our observations suggest that cardiomyocytes start to extend protrusions before they begin entering the trabecular layer, but it is not clear how they actually translocate from the compact layer into the forming trabecular layer. To address this, we generated high-resolution time-lapse movies using a different technique to image the developing hearts. In brief, *Tg(myl7:ras-GFP)* fish mosaically labeled as above were anesthetized to the point where their heart stopped beating. After acquiring *z*-stacks of the stopped ventricles, we washed out the anesthetic, at which time the hearts began to beat again. Hearts were then allowed to develop 3-4 hours before being stopped again. The high-resolution images thereby obtained allowed us to unambiguously identify individual cardiomyocytes as they entered the trabecular layer. We found that cardiomyocytes progressively constricted their abluminal surface, eventually exiting the compact layer (Fig. 3A-E′). Interestingly, we observed cardiomyocytes extending new protrusions as they constricted their abluminal surface (Fig. 3C-H′). The total volume of each of these cardiomyocytes remained relatively constant, suggesting that they redistribute their abluminal volume into the new expanding protrusions (Fig. 3F-H′).

To examine this process further, we returned to imaging beating hearts. We first imaged cardiomyocytes in transverse section as they entered the trabecular layer (red cardiomyocyte in Fig. 4A; supplementary material Movie 5). We found that cardiomyocytes gradually constricted their abluminal surface and exited the compact layer over several hours. As mentioned above, cardiomyocytes entering the trabecular layer concurrently extended protrusions into the trabecular layer while constricting their abluminal surface (green
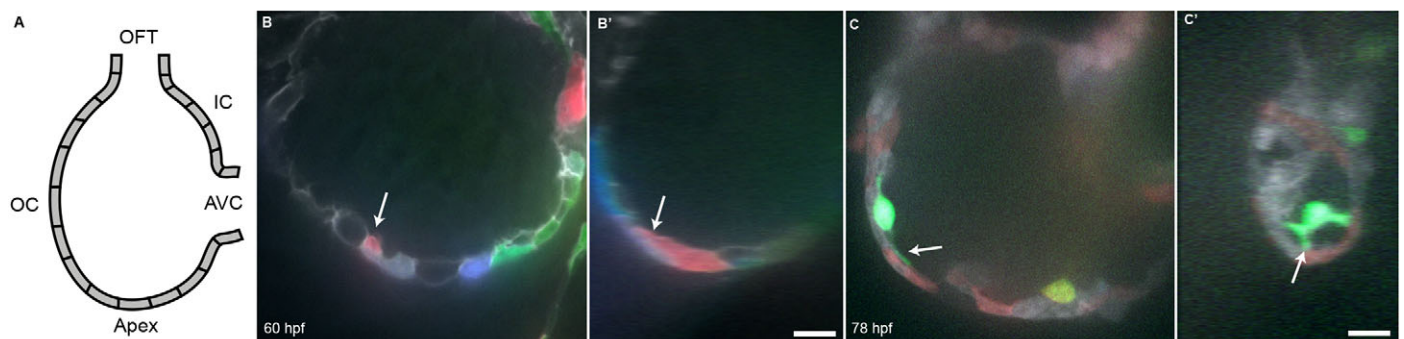
Fig. 2. Cardiomyocytes extend protrusions luminally while still in the compact layer. (A) Illustration of the orientation of the hearts shown in B and C. (B) Optical slice of a 60 hpf *Tg(myl7:ras-GFP)* heart with cardiomyocytes marked with multiple fluorescent proteins. Arrow points to a marked cellular protrusion (red), extending over another marked cardiomyocyte (purple). (B′) View of the same dataset as B rotated 90°, showing that this protrusion extends from a cardiomyocyte that is still mostly contained within the compact layer. (C) Optical slice of a 78 hpf *Tg(myl7:EGFP)* heart similarly marked with multiple fluorescent proteins. Arrow points to a protrusion extending from a trabecular cardiomyocyte (green). (C′) View of the same dataset as C rotated 90°, showing that the same cardiomyocyte extends multiple protrusions. AVC, atrioventricular canal; IC, inner curvature; OC, outer curvature; OFT, outflow tract. Scale bars: 10 μm.

Fig. 3. Cardiomyocytes show evidence of abluminal constriction. (A) 3D exterior view of a 72 hpf *Tg(myl7:ras-GFP)* heart with a subset of cardiomyocytes randomly labeled with RFP. Membrane GFP signal is pseudocolored white, and mosaically marked cardiomyocytes are in red. A cardiomyocyte of interest is highlighted in purple. (B) Interior chamber view of the same heart. Cardiomyocyte of interest is highlighted in purple. (C-E) Time-lapse highlighting a cardiomyocyte of interest in another heart. A single *xy* plane is shown at the start of imaging (C), at +3 hours of imaging (D), and at +6 hours of imaging (E). Orientation is as in A. Dotted lines outline the gradually constricting cell contact with the abluminal surface. The neighboring cardiomyocytes are highlighted in yellow and green. In E, the cardiomyocyte has lost contact with the abluminal surface and thus can no longer be seen. (C′-E′) Re-slice of the confocal stack showing the same cardiomyocyte rotated 90°. Cardiomyocyte of interest is highlighted in purple, and neighboring cardiomyocytes are in yellow and green. The cardiomyocyte can be seen extending a protrusion (arrowheads) as it exits the compact layer. (F-H) 3D volume rendering of the highlighted cardiomyocyte. Arrows point to contracting contact with the abluminal surface. Arrowheads point to the extending protrusion shown in E′. (F′-H′) 90° rotation of F-H showing luminal view of the cardiomyocyte. Scale bars: 10 µm in A-E; 5 µm in F-H′.

cardiomyocyte in Fig. 4B,C, arrow in 4C; supplementary material Movie 6). Notably, although we could identify very occasional cardiomyocyte divisions within our time-lapse movies (1/103 clonally labeled cardiomyocytes observed; supplementary material Fig. S1, Movie 7), all cardiomyocytes observed entering the trabecular layer did so without undergoing cell division. Interestingly, in several cases, cardiomyocytes neighboring trabeculating cardiomyocytes exhibited dramatic cell shape changes, allowing them to fill the space vacated by the exiting cardiomyocyte (e.g. purple cardiomyocyte in Fig. 4B,C; supplementary material Movie 6).

Trabeculation-deficient animals exhibit different modes of trabecular failure

A number of mutants have been identified to exhibit defects in trabeculation (Gassmann et al., 1995; Lee et al., 1995; Meyer and Birchmeier, 1995; Kramer et al., 1996; Suri et al., 1996; Jones et al., 2003; Liu et al., 2010; Peshkovsky et al., 2011). However, the affected cellular behaviors underlying the trabecular defects remain undefined. To determine how changes in cardiomyocyte behaviors lead to defects in trabeculation, we examined three models of trabecular failure in zebrafish: *tnnt2a* morphants, *myh6* morphants
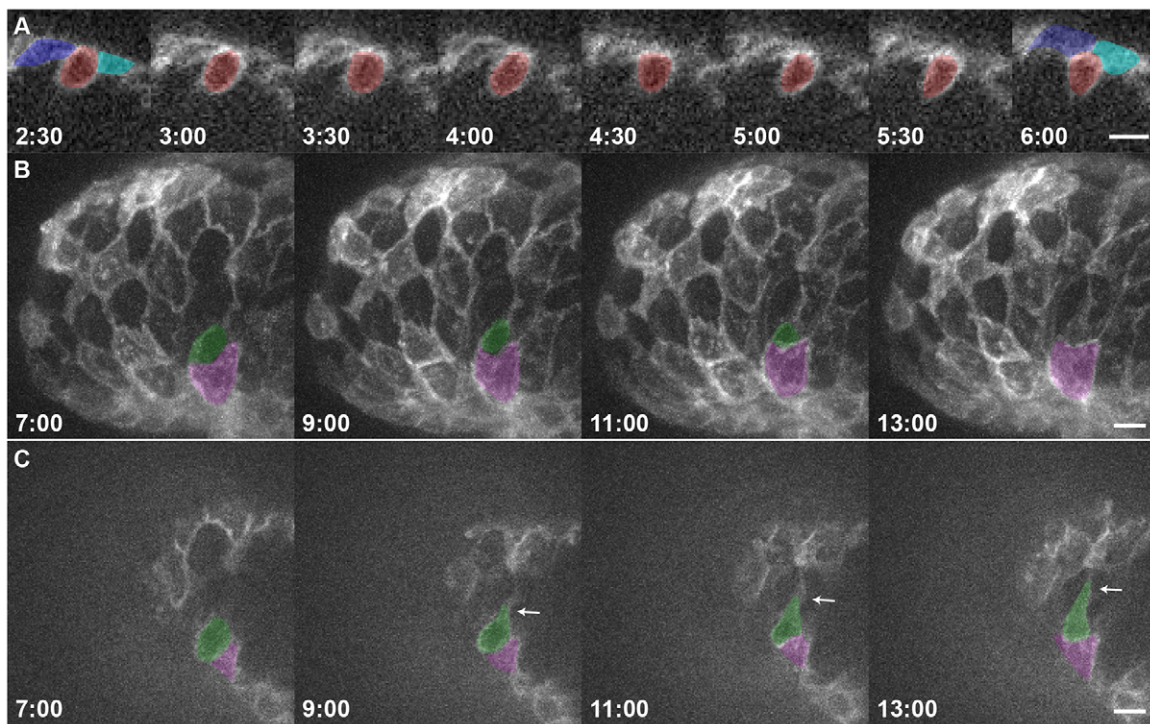
Fig. 4. Cardiomyocytes extend protrusions while constricting their abluminal surface. (A) Transverse section of a *Tg(myl7:ras-GFP)* heart imaged starting at 60 hpf showing a cardiomyocyte entering the trabecular layer (red). The neighboring cardiomyocytes are marked in blue and cyan at the beginning and end of the movie. Note the increase over time in *Tg(myl7:ras-GFP)* signal abluminal to the marked cardiomyocyte. This increase appears to be caused by the movement of neighboring cardiomyocytes. (B) 3D projection of a *Tg(myl7:ras-GFP)* heart imaged starting at 59 hpf. Time from start of imaging (hours:minutes) is shown on lower left. The cardiomyocyte marked in green constricts its abluminal surface. This cardiomyocyte completely exits the compact layer by 13 hours of imaging. The cardiomyocyte marked in purple changes shape to take up part of the space vacated by the green cardiomyocyte. (C) Drift-corrected (see Materials and Methods) optical slice 15 μm from the abluminal surface of the heart shown in B. Green and purple cardiomyocytes from B are marked accordingly. The green cardiomyocyte extends a protrusion luminally (arrows). Scale bars: 10 μm.

and *erbb2* mutants. Consistent with previous observations, we never observed myocardial cell bodies enter the trabecular layer in these embryos during our live imaging analysis. Thus, we looked earlier, at the initial formation of trabecular protrusions. To examine protrusions in a quantitative manner, we performed clonal analysis in wild-type and trabeculation-deficient embryos via the transient transgenesis approaches outlined above, and imaged the marked cardiomyocytes over a 10-hour period. Cardiomyocytes were scored for extension of protrusions (Fig. 5A), number of protrusions extended (Fig. 5B), and for whether protrusions persisted over the entire 10-hour imaging period (Fig. 5C).

We and others have previously shown that the ErbB2 receptor tyrosine kinase is necessary for trabecular development in both mouse and zebrafish (Gassmann et al., 1995; Lee et al., 1995; Meyer and Birchmeier, 1995; Kramer et al., 1996; Jones et al., 2003; Lai et al., 2010; Liu et al., 2010; Peshkovsky et al., 2011). We have also shown that *erbb2* mutant cardiomyocytes exhibit a cell-autonomous defect in trabeculation (Liu et al., 2010). However, the cellular mechanisms that cause this defect remain unknown. Strikingly, cardiomyocytes in *erbb2* mutants were less likely to extend protrusions than wild-type cardiomyocytes, with 29% of *erbb2* mutant cardiomyocytes extending protrusions compared with 48% of wild-type cardiomyocytes (Fig. 5D; *P*=0.04). *erbb2* mutant cardiomyocytes also extended an average of 1.06 protrusions/cardiomyocyte, compared with 1.28 in wild type (Fig. 5E; *P*=0.03). Additionally, *erbb2* mutant protrusions tended to be less stable, with 58% of protrusions collapsing within the 10-hour imaging period compared with only 21% in wild type (Fig. 5F;

P=0.07). Thus, lack of ErbB2 function seems to inhibit the initial formation of protrusions and may decrease their stability as well.

Contractility and/or blood flow play an important role in cardiac development (Berdougo et al., 2003; Bartman et al., 2004; Chi et al., 2008; Vermot et al., 2009; Chi et al., 2010; Peshkovsky et al., 2011), and have specifically been implicated in trabecular development (Chi et al., 2008; Peshkovsky et al., 2011). Notably, *tnnt2a* mutant hearts, which fail to form functional sarcomeres and thus fail to contract (Sehnert et al., 2002), do not form trabeculae (Chi et al., 2008). However, since both contractility and blood flow are disrupted in *tnnt2a* mutants, it is difficult to separate out the role that each might play in trabeculation. Interestingly, *weak atrium* (*myh6*) mutants, which exhibit disrupted atrial contraction and thus reduced blood flow through the ventricle, also have defects in trabeculation (Peshkovsky et al., 2011). To study the role that physical forces play in trabeculation, we performed clonal analysis in embryos injected with morpholinos targeting *tnnt2a* or *myh6*, which phenocopy the respective mutants (Sehnert et al., 2002; Berdougo et al., 2003). The two morphants exhibited different phenotypes in terms of their myocardial protrusions. In *tnnt2a* morphants, a similar number of cardiomyocytes extended protrusions as in wild type (52% in *tnnt2a* morphants versus 48% in wild type, *P*=0.8), but the protrusions were less stable and retracted more frequently (62% retracting in *tnnt2a* morphants versus 21% in wild type, *P*=0.02). By contrast, in *myh6* morphants, the cardiomyocytes showed a trend towards extending fewer protrusions than in wild type (24% in *myh6* morphant versus 48% in wild type, *P*=0.07), but the protrusions they did extend were as stable as in wild type (16% retracting in *myh6*
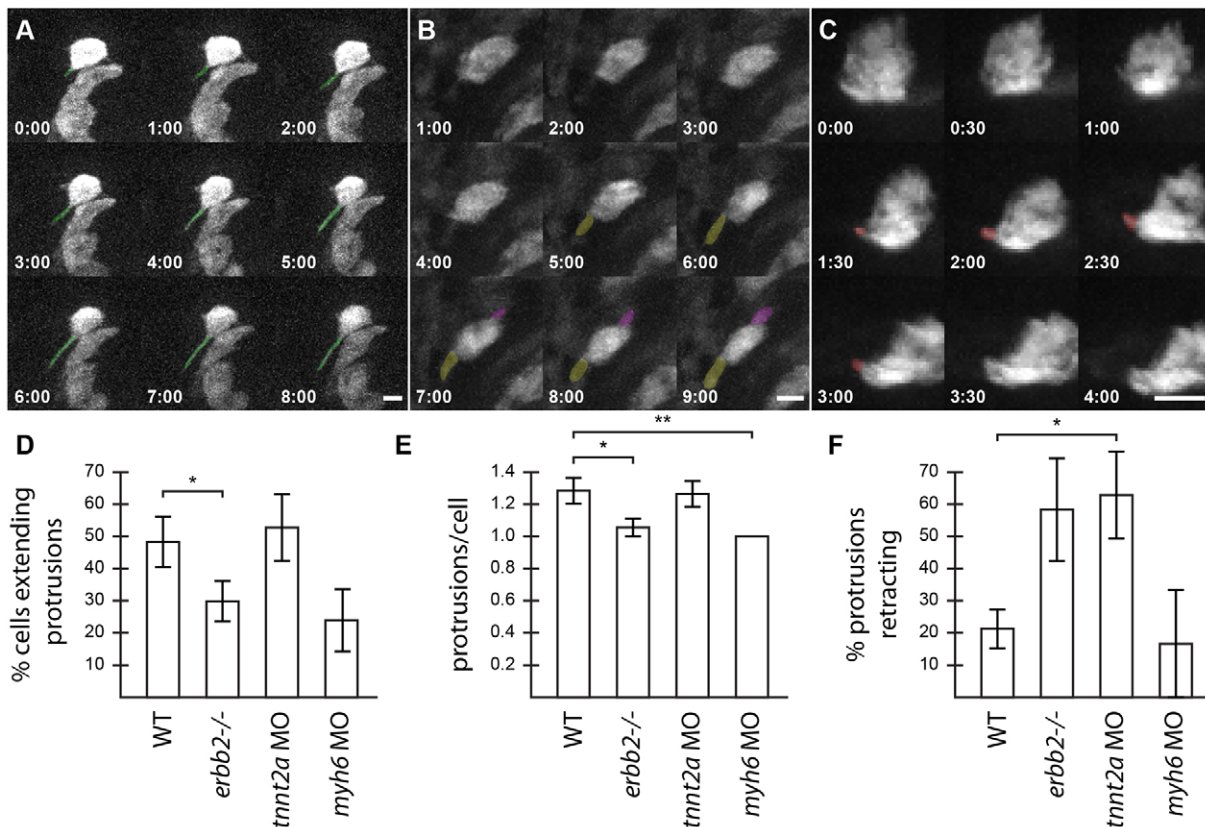
Fig. 5. Trabecular-deficient animals exhibit different modes of trabecular failure. (A-C) Examples of distinct cardiomyocyte behavior: (A) a cardiomyocyte extending a single protrusion (green); (B) a cardiomyocyte extending two protrusions (purple and yellow); and (C) a cardiomyocyte extending a protrusion which then retracts over the next 2 hours (red). Scale bars: 10 μm. (D-F) Quantification of the properties and behavior of myocardial protrusions in trabecular-deficient backgrounds. Error bars indicate s.e.m. Data were collected from 97 WT cells (14 embryos, 59 processes), 40 *tnnt2a* morphant cells (seven embryos, 32 processes), 37 *erbb2* mutant cells (six embryos, 14 processes) and 20 *amhc* morphant cells (four embryos, eight processes). (D) The number of cardiomyocytes extending protrusions as a proportion of the total number of cardiomyocytes counted. (E) The number of protrusions per cardiomyocyte that extended at least one protrusion. (F) The number of protrusions that retracted in length during a 10-hour movie, as a proportion of the total number of protrusions observed in each set of embryos. *$P<0.05$, **$P<0.005$. WT, wild type.

morphants versus 21% in wild type, $P=0.81$). Notably, whereas wild-type cardiomyocytes occasionally extended more than one protrusion per cell (average of 1.28 protrusions/cardiomyocyte in wild type), the cardiomyocytes in *myh6* morphants uniformly extended only one protrusion ($P=0.004$).

DISCUSSION

In this study, we combined clonal analysis with powerful live imaging techniques to identify myocardial cell behaviors leading to trabeculation. We identified a previously unknown capability of actively contracting cardiomyocytes to extend long luminal protrusions, even before they translocate to form the trabeculae. Further, our data show that cardiomyocytes enter the trabecular layer through abluminal constriction, extending protrusions as they enter. While cardiomyocytes constrict their abluminal surface and enter the trabecular layer, neighboring cardiomyocytes move into the space left behind to maintain a cohesive compact layer. Finally, we found that cardiomyocytes in non-contractile hearts fail to stabilize their protrusions, which is likely to contribute to their failure to form trabeculae, and that cardiomyocytes in *erbb2* mutants fail to form trabeculae despite forming stable, though fewer, protrusions.

Previous studies in zebrafish have shown that cardiomyocytes change shape depending on their location within the heart (Auman et al., 2007; Chi et al., 2010; Lin et al., 2012). However, given the

necessity to maintain the integrity of the myocardial epithelium, it has been generally assumed that it was a very stable and static structure. Thus, it was surprising to find that cardiomyocytes exhibit such a dynamic behavior. The combination of live imaging, clonal analysis and image processing allowed us to reveal this process for the first time. How trabecular and compact layer cardiomyocytes are specified remains unknown. The identification of myocardial protrusions that invade luminally before cardiomyocytes translocate into the trabecular layer raises a number of hypotheses about their function. The early extension of protrusions could allow cardiomyocytes to sample their environment, seeking limiting supplies of fate-determining morphogens for example. In addition, these protrusions could provide cardiomyocytes with extra space to redistribute their volume as they constrict their abluminal surface. Interestingly, we noted that cardiomyocyte protrusions preferentially extend over cell-cell junctions of the compact layer. This arrangement could provide a mechanism for strengthening weak attachments or aligning cytoskeletons among multiple cardiomyocytes.

The ventricular trabeculae form an intricate, interconnected network in zebrafish (Sedmera et al., 2003; Chi et al., 2008; Peshkovsky et al., 2011), as well as in chick, mouse and human (Sedmera et al., 2000). How cardiomyocytes interact to form this network is poorly understood. In theory, the trabecular network

organization could form in two broad ways. Trabecular ridges could be specified in the compact layer, and multiple neighboring cardiomyocytes could translocate to the trabecular layer to form a pre-assembled ridge. Alternatively, trabecular cardiomyocytes could be specified intermittently throughout the compact layer and form new connections with other trabecular cardiomyocytes to create the trabecular network. Our live imaging identified instances in which protrusions from two non-neighboring cardiomyocytes came together to form a new contact between the cells. Although the role of these new contacts remains to be explored, this observation provides a clue that the trabecular network could form through the assembly of new cell-cell connections within the forming trabecular layer.

Our previous work had suggested that trabeculation involves cardiomyocyte migration, rather than oriented cell division (Liu et al., 2010), although the exact mechanisms of migration remained unknown. Our live imaging of cardiomyocyte delamination reveals that cardiomyocytes enter the trabecular layer via constriction of their abluminal surface, coupled to a redistribution of their cell volume into luminal protrusions. Importantly, cell divisions were never seen to accompany this migration, confirming that delamination is independent of cardiomyocyte proliferation. The abluminal constriction of cardiomyocytes resembles the process of apical constriction, which is involved in a number of important morphogenetic events (Sawyer et al., 2010). Indeed, if the apical domain of cardiomyocytes remains unchanged from the 20-somite stage, when it faces away from the endocardium (Trinh and Stainier, 2004; Trinh et al., 2005), this process might represent apical constriction.

Delamination following apical constriction has been observed in a number of different systems. Generally, there are two non-exclusive mechanisms that can drive cellular constriction and delamination. First, delaminating cells can constrict their own apical surface through actin rearrangements and myosin-mediated contraction, as observed in *C. elegans* gastrulation (Lee et al., 2006). Second, their neighbors could coordinate to form an actin ring to extrude the delaminating cardiomyocyte out of the compact layer, as is seen in crowding-induced delamination from the fly notum (Marinari et al., 2012). The combination of these two mechanisms has also been observed in the extrusion of apoptotic cells from epithelial layers (Rosenblatt et al., 2001; Slattum et al., 2009; Gu et al., 2011). Our study cannot distinguish between these three possibilities. Our previous study has shown that trabeculation can be inhibited cell-autonomously (Liu et al., 2010), although this finding cannot rule out a mechanism in which delaminating cardiomyocytes signal to their neighbors to form a contractile ring. Additionally, it is currently unclear whether compact cardiomyocytes rearrange to occupy the space left behind by their delaminating neighbors by changing their morphology, migrating, rearranging their cell junctions or through some other mechanism. Further studies are needed to clarify the precise roles of future trabecular cardiomyocytes and their neighbors during the delamination process.

In confirmation of previous studies, we observed that cardiomyocytes in *erbb2* mutants, or in *tnnt2a* or *myh6* morphants, fail to delaminate into the trabecular layer, at least during the stages that we imaged. However, we wished to determine whether the mechanisms leading to trabecular failure differed between these deficient states. Using a combination of clonal analysis and live imaging, we were able to extend our analysis to look at whether these deficiencies differentially affected the formation of myocardial protrusions. Interestingly, each of these three manipulations affected the protrusions differently. A mutation in *erbb2* led to roughly half

as many cardiomyocytes extending protrusions, and perhaps also to less stable protrusions. This suggests that *erbb2* contributes to the formation of protrusions and perhaps to their stability. Combined with our previous finding that *erbb2* is necessary for cardiomyocyte proliferation during zebrafish development (Liu et al., 2010), these data suggest that *erbb2* mutants have deficiencies in the initiation of trabeculation as well as in the subsequent growth of these structures.

Injection of morpholinos that change the mechanical environment of the heart produces notably different effects on the myocardial protrusions. Comparing the *tnnt2a* and *myh6* morphants provides an opportunity to distinguish the effects of blood flow from those of contractility on trabecular development. The notable instability of the protrusions in *tnnt2a* morphants, as compared with the relatively unaffected stability in *myh6* morphants, suggests that contractility and/or the contractile structures themselves contribute to the stability of the protrusions. Paradoxically, decreasing blood flow through the ventricle via the *myh6* morpholino actually decreases the number of protrusions that cardiomyocytes extend, whereas no difference from wild type is noted in the *tnnt2a* morphants. Although there are many possible explanations for these seemingly conflicting observations, we currently favor a model in which sarcomeres stabilize protrusions at their current length, preventing either collapse or further extension. Dynamic rearrangements in sarcomeric structures can thus modulate the extension or collapse of protrusions. In *erbb2* mutant cardiomyocytes, actin appears to be sequestered in, or around, sarcomeric pools compared with wild type (S. Reischauer and D.Y.R.S., unpublished observations). This sequestration might decrease the frequency of myocardial protrusions. Previous work has shown that *myh6* mutant cardiomyocytes have an altered sarcomere distribution (Lin et al., 2012). This altered sarcomeric pattern might negatively impact the extension of myocardial protrusions. In *tnnt2a* morphants, the cardiomyocytes cannot make sarcomeres and thus their protrusions extend without 'inhibition', but also cannot be stabilized. Additional reagents and experiments will be required to test these hypotheses.

In conclusion, our study demonstrates the power of combining clonal analysis and live imaging to probe cardiac development in zebrafish. Expanding this approach will provide a unique tool to address *in vivo* further cell biological questions during the development of the heart and other fast-moving tissues.

MATERIALS AND METHODS
Zebrafish and morpholino injections
Embryonic and adult zebrafish were maintained according to standard laboratory conditions (Westerfield, 2000) and IACUC license. We used the following transgenic and mutant lines: *Tg(myl7:ras-eGFP)^s883* (D'Amico et al., 2007) and *erbb2^st61* (Lyons et al., 2005; Liu et al., 2010). To generate *tnnt2a* and *myh6* morphants, 1.2 ng *tnnt2a* morpholino (5′-CATGTTTGCTCTGATCTGACACGCA-3′) or 1.2 ng *myh6* morpholino (5′-ACTCTGCCATTAAAGCATCACCCAT-3′) was injected in 1 nl total volume into the yolk of single-cell stage embryos.

Mosaic analyses
DNA constructs based on the miniTol2 vector (Balciunas et al., 2006) harboring a *myl7* promoter (Huang et al., 2003) upstream of TagRFP-T (Shaner et al., 2008), TagBFP (Subach et al., 2008) or IRFP (Filonov et al., 2011) were constructed using the Cold Fusion Cloning Kit (SBI, MC100B-1). For single-color mosaic analysis, 1 nl of a mixture of *myl7:TagRFP-T* plasmid at 5-10 ng/µl and Tol2 RNA at 25 ng/µl was injected into *Tg(myl7:ras-eGFP)^s883* embryos. For multi-color mosaic analysis, three different DNA constructs each at 5-10 ng/µl were co-injected with 25 ng/µl Tol2 RNA. Embryos were screened for fluorescence and normal morphology at 55 hpf before being selected for imaging.

Imaging

Live imaging of heart development

Embryos at 55-60 hpf were mounted in 1% low-melting agarose supplemented with 0.015% (w/v) tricaine on glass-bottom dishes (MatTek, P35G-0-20-C). Embryos were mounted slightly tilted on their right side so that the ventricle was closest to the coverslip. Movies of live zebrafish hearts were acquired using a Nikon Ti-E inverted microscope with a Yokagawa CSU-22 spinning disk head using either a 20×/0.75 air objective (Nikon) or a 40×/1.15 water immersion objective. For movies taken with the 20× lens, a 1.5× multiplier lens was added to the light path. Movies were recorded using an Evolve EMCCD camera (Photometrics). To achieve the acquisition rate of 60 frames per second, the camera was binned 2×2, yielding a calculated pixel resolution of 0.61 (20× objective/1.5× multiplier) or 0.455 (40×/1.15 objective) μm/pixel. We used the following laser lines: 405 nm (100 mW Coherent Cube Diode), 491 nm (100 mW Cobolt Calypso DPSS), 561 nm (100 mW Coherent Sapphire DPSS) and 640 nm (100 mW Coherent Cube Diode). Emission filters used were TagBFP (460±25 nm), GFP (525±25 nm), TagRFP-T (610±30 nm) and IRFP (700±38 nm). To reduce laser exposure and motion blur, lasers were pulsed for 2-5 ms/frame using an Acousto-Optic Tunable Filter (Neos) gated on the camera trigger. Multiple embryos were imaged using a motorized stage (Prior). The microscope was controlled using μManager (Edelstein et al., 2010), and z-translation of the heart was corrected live using a custom script. To increase the rate of development, the imaging environment was heated to 31°C using a thermally controlled enclosure (In Vivo Scientific). Generally, movies of 90 frames each were collected at 50 z-positions 1 μm apart for each developmental time point. Developmental time points were collected every 15-30 minutes for 12-19 hours, depending on the experiment. The assembled datasets were then temporally aligned using previously published Matlab software (Liebling et al., 2005; Liebling et al., 2006; Ohn et al., 2009), and the aligned files were viewed and analyzed in Fiji (Schindelin et al., 2012).

Quantitation of protrusions

Cardiomyocytes were mosaically labeled as described above in wild type, *erbb2* mutants, *tnnt2a* morphants or *myh6* morphants and imaged live for 10 hours. To identify *erbb2* mutants before imaging, embryos were sorted according to a tail phenotype consisting of a pointed caudal fin and a poorly formed 'wavy' dorsal fin. Genotype was subsequently confirmed by PCR (Lyons et al., 2005). 3D movies from ventricular diastole were manually identified for each embryo. z-projections were generated from each 3D movie, and the filenames were randomized to enable blinded scoring. Each 3D movie was scored for (1) the number of countable cardiomyocytes, (2) the number of cardiomyocytes extending protrusions, (3) the total number of protrusions and (4) the number of protrusions that retracted. Cardiomyocytes were deemed scorable if their edges were clearly distinct from the next closest cardiomyocyte. Protrusions were defined as subdomains of cardiomyocytes that had a clearly identifiable base and were more than 2 μm in length at some point in the movie and changed throughout the 10-hour movie. Protrusions were counted as retracting if their length began decreasing and reduced to less than one half of their maximal length during the course of the movie. The original z-stack was used to confirm the presence or absence of protrusions. The number of protrusions per cardiomyocyte, the percentage of cardiomyocytes extending protrusions, and percentage of protrusions that retracted were calculated for each embryo, and the various mutants and morphants were compared with wild type using a two-tailed t-test.

Periodic stopped heart imaging

Embryos were mounted in agarose as above, then anesthetized to the point of cardioplegia with 0.2% tricaine. A z-stack was then acquired on the microscope described above using a 40×/1.15 water immersion objective (Nikon). In this case, the camera was not binned, yielding a calculated resolution of 227.5 nm/pixel. The anesthetic was then washed out, and the embryos were monitored until the heart resumed normal beating. To increase the rate of development, embryos were then incubated at 31°C for 3 hours, at which time anesthetic was reapplied to induce cardioplegia, and the process repeated. Each dataset consisted of four separate time points. The cardiac health of the embryos was visually assessed after imaging to ensure normal function.

Imaging of stopped hearts

Embryos were mounted in 1% agarose containing 0.2% (w/v) tricaine. Embryos were then imaged using a Zeiss LSM5 confocal microscope.

Image processing

Most 3D datasets were rendered in Fiji using the Z projection tool or the 3D Viewer plugin. When noted, surface renderings were created in Imaris (Bitplane). When a noticeable drift in the x, y or z dimension was noticed, it was corrected using the Correct 3D Drift plugin in Fiji. In some instances, the StackReg plugin (Fiji) was used on the time-lapse of z-projections to allow better analysis of individual cardiomyocytes.

Supplementary material

Supplementary material available online at
http://dev.biologists.org/lookup/suppl/doi:10.1242/dev.098632/-/DC1

References

Auman, H. J., Coleman, H., Riley, H. E., Olale, F., Tsai, H. J. and Yelon, D. (2007). Functional modulation of cardiac form through regionally confined cell shape changes. *PLoS Biol.* **5**, e53.

Balciunas, D., Wangensteen, K. J., Wilber, A., Bell, J., Geurts, A., Sivasubbu, S., Wang, X., Hackett, P. B., Largaespada, D. A., McIvor, R. S. et al. (2006). Harnessing a high cargo-capacity transposon for genetic applications in vertebrates. *PLoS Genet.* **2**, e169.

Bartman, T., Walsh, E. C., Wen, K. K., McKane, M., Ren, J., Alexander, J., Rubenstein, P. A. and Stainier, D. Y. R. (2004). Early myocardial function affects endocardial cushion development in zebrafish. *PLoS Biol.* **2**, E129.

Beis, D. and Stainier, D. Y. R. (2006). In vivo cell biology: following the zebrafish trend. *Trends Cell Biol.* **16**, 105-112.

Berdougo, E., Coleman, H., Lee, D. H., Stainier, D. Y. R. and Yelon, D. (2003). Mutation of weak atrium/atrial myosin heavy chain disrupts atrial function and influences ventricular morphogenesis in zebrafish. *Development* **130**, 6121-6129.

Chi, N. C., Shaw, R. M., Jungblut, B., Huisken, J., Ferrer, T., Arnaout, R., Scott, I., Beis, D., Xiao, T., Baier, H. et al. (2008). Genetic and physiologic dissection of the vertebrate cardiac conduction system. *PLoS Biol.* **6**, e109.

Chi, N. C., Bussen, M., Brand-Arzamendi, K., Ding, C., Olgin, J. E., Shaw, R. M., Martin, G. R. and Stainier, D. Y. R. (2010). Cardiac conduction is required to preserve cardiac chamber morphology. *Proc. Natl. Acad. Sci. USA* **107**, 14662-14667.

D'Amico, L., Scott, I. C., Jungblut, B. and Stainier, D. Y. R. (2007). A mutation in zebrafish hmgcr1b reveals a role for isoprenoids in vertebrate heart-tube formation. *Curr. Biol.* **17**, 252-259.

Edelstein, A., Amodaj, N., Hoover, K., Vale, R. and Stuurman, N. (2010). Computer control of microscopes using μManager. *Curr. Protoc. Mol. Biol.* **92**, 14.20.1-14.20.17.

Filonov, G. S., Piatkevich, K. D., Ting, L.-M., Zhang, J., Kim, K. and Verkhusha, V. V. (2011). Bright and stable near-infrared fluorescent protein for in vivo imaging. *Nat. Biotechnol.* **29**, 757-761.

Gassmann, M., Casagranda, F., Orioli, D., Simon, H., Lai, C., Klein, R. and Lemke, G. (1995). Aberrant neural and cardiac development in mice lacking the ErbB4 neuregulin receptor. *Nature* **378**, 390-394.

Gu, Y., Forostyan, T., Sabbadini, R. and Rosenblatt, J. (2011). Epithelial cell extrusion requires the sphingosine-1-phosphate receptor 2 pathway. *J. Cell Biol.* **193**, 667-676.

Gupta, V. and Poss, K. D. (2012). Clonally dominant cardiomyocytes direct heart morphogenesis. *Nature* **484**, 479-484.

Huang, C.-J., Tu, C.-T., Hsiao, C.-D., Hsieh, F.-J. and Tsai, H.-J. (2003). Germ-line transmission of a myocardium-specific GFP transgene reveals critical regulatory elements in the cardiac myosin light chain 2 promoter of zebrafish. *Dev. Dyn.* **228**, 30-40.

Jenni, R., Rojas, J. and Oechslin, E. (1999). Isolated noncompaction of the myocardium. *N. Engl. J. Med.* **340**, 966-967.

Jones, F. E., Golding, J. P. and Gassmann, M. (2003). ErbB4 signaling during breast and neural development: novel genetic models reveal unique ErbB4 activities. *Cell Cycle* **2**, 555-559.

Kawakami, K. (2007). Tol2: a versatile gene transfer vector in vertebrates. *Genome Biol.* **8** Suppl 1, S7.

Kramer, R., Bucay, N., Kane, D. J., Martin, L. E., Tarpley, J. E. and Theill, L. E. (1996). Neuregulins with an Ig-like domain are essential for mouse myocardial and neuronal development. *Proc. Natl. Acad. Sci. USA* **93**, 4833-4838.

Lai, D., Liu, X., Forrai, A., Wolstein, O., Michalicek, J., Ahmed, I., Garratt, A. N., Birchmeier, C., Zhou, M., Hartley, L. et al. (2010). Neuregulin 1 sustains the gene regulatory network in both trabecular and nontrabecular myocardium. *Circ. Res.* **107**, 715-727.

Lee, K.-F., Simon, H., Chen, H., Bates, B., Hung, M.-C. and Hauser, C. (1995). Requirement for neuregulin receptor erbB2 in neural and cardiac development. *Nature* **378**, 394-398.

Lee, J.-Y., Marston, D. J., Walston, T., Hardin, J., Halberstadt, A. and Goldstein, B. (2006). Wnt/Frizzled signaling controls C. elegans gastrulation by activating actomyosin contractility. *Curr. Biol.* **16**, 1986-1997.

Liebling, M., Forouhar, A. S., Gharib, M., Fraser, S. E. and Dickinson, M. E. (2005). Four-dimensional cardiac imaging in living embryos via postacquisition synchronization of nongated slice sequences. *J. Biomed. Opt.* **10**, 054001.

Liebling, M., Forouhar, A. S., Wolleschensky, R., Zimmermann, B., Ankerhold, R., Fraser, S. E., Gharib, M. and Dickinson, M. E. (2006). Rapid three-dimensional imaging and analysis of the beating embryonic heart reveals functional changes during development. *Dev. Dyn.* **235**, 2940-2948.

Lin, Y.-F., Swinburne, I. and Yelon, D. (2012). Multiple influences of blood flow on cardiomyocyte hypertrophy in the embryonic zebrafish heart. *Dev. Biol.* **362**, 242-253.

Liu, J., Bressan, M., Hassel, D., Huisken, J., Staudt, D., Kikuchi, K., Poss, K. D., Mikawa, T. and Stainier, D. Y. R. (2010). A dual role for ErbB2 signaling in cardiac trabeculation. *Development* **137**, 3867-3875.

Lyons, D. A., Pogoda, H.-M., Voas, M. G., Woods, I. G., Diamond, B., Nix, R., Arana, N., Jacobs, J. and Talbot, W. S. (2005). erbb3 and erbb2 are essential for schwann cell migration and myelination in zebrafish. *Curr. Biol.* **15**, 513-524.

Marinari, E., Mehonic, A., Curran, S., Gale, J., Duke, T. and Baum, B. (2012). Live-cell delamination counterbalances epithelial growth to limit tissue overcrowding. *Nature* **484**, 542-545.

Meilhac, S. M., Kelly, R. G., Rocancourt, D., Eloy-Trinquet, S., Nicolas, J.-F. and Buckingham, M. E. (2003). A retrospective clonal analysis of the myocardium reveals two phases of clonal growth in the developing mouse heart. *Development* **130**, 3877-3889.

Meilhac, S. M., Esner, M., Kerszberg, M., Moss, J. E. and Buckingham, M. E. (2004a). Oriented clonal cell growth in the developing mouse myocardium underlies cardiac morphogenesis. *J. Cell Biol.* **164**, 97-109.

Meilhac, S. M., Esner, M., Kelly, R. G., Nicolas, J.-F. and Buckingham, M. E. (2004b). The clonal origin of myocardial cells in different regions of the embryonic mouse heart. *Dev. Cell* **6**, 685-698.

Meyer, D. and Birchmeier, C. (1995). Multiple essential functions of neuregulin in development. *Nature* **378**, 386-390.

Mikawa, T., Borisov, A., Brown, A. M. and Fischman, D. A. (1992). Clonal analysis of cardiac morphogenesis in the chicken embryo using a replication-defective retrovirus: I. Formation of the ventricular myocardium. *Dev. Dyn.* **193**, 11-23.

Morris, J. K., Lin, W., Hauser, C., Marchuk, Y., Getman, D. and Lee, K. F. (1999). Rescue of the cardiac defect in ErbB2 mutant mice reveals essential roles of ErbB2 in peripheral nervous system development. *Neuron* **23**, 273-283.

Ohn, J., Tsai, H.-J. and Liebling, M. (2009). Joint dynamic imaging of morphogenesis and function in the developing heart. *Organogenesis* **5**, 248-255.

Peshkovsky, C., Totong, R. and Yelon, D. (2011). Dependence of cardiac trabeculation on neuregulin signaling and blood flow in zebrafish. *Dev. Dyn.* **240**, 446-456.

Rosenblatt, J., Raff, M. C. and Cramer, L. P. (2001). An epithelial cell destined for apoptosis signals its neighbors to extrude it by an actin- and myosin-dependent mechanism. *Curr. Biol.* **11**, 1847-1857.

Sawyer, J. M., Harrell, J. R., Shemer, G., Sullivan-Brown, J., Roh-Johnson, M. and Goldstein, B. (2010). Apical constriction: a cell shape change that can drive morphogenesis. *Dev. Biol.* **341**, 5-19.

Schindelin, J., Arganda-Carreras, I., Frise, E., Kaynig, V., Longair, M., Pietzsch, T., Preibisch, S., Rueden, C., Saalfeld, S., Schmid, B. et al. (2012). Fiji: an open-source platform for biological-image analysis. *Nat. Methods* **9**, 676-682.

Sedmera, D., Pexieder, T., Rychterova, V., Hu, N. and Clark, E. B. (1999). Remodeling of chick embryonic ventricular myoarchitecture under experimentally changed loading conditions. *Anat. Rec.* **254**, 238-252.

Sedmera, D., Pexieder, T., Vuillemin, M., Thompson, R. P. and Anderson, R. H. (2000). Developmental patterning of the myocardium. *Anat. Rec.* **258**, 319-337.

Sedmera, D., Reckova, M., deAlmeida, A., Sedmerova, M., Biermann, M., Volejnik, J., Sarre, A., Raddatz, E., McCarthy, R. A., Gourdie, R. G. et al. (2003). Functional and morphological evidence for a ventricular conduction system in zebrafish and Xenopus hearts. *Am. J. Physiol.* **284**, H1152-H1160.

Sehnert, A. J., Huq, A., Weinstein, B. M., Walker, C., Fishman, M. and Stainier, D. Y. R. (2002). Cardiac troponin T is essential in sarcomere assembly and cardiac contractility. *Nat. Genet.* **31**, 106-110.

Shaner, N. C., Lin, M. Z., McKeown, M. R., Steinbach, P. A., Hazelwood, K. L., Davidson, M. W. and Tsien, R. Y. (2008). Improving the photostability of bright monomeric orange and red fluorescent proteins. *Nat. Methods* **5**, 545-551.

Slattum, G., McGee, K. M. and Rosenblatt, J. (2009). P115 RhoGEF and microtubules decide the direction apoptotic cells extrude from an epithelium. *J. Cell Biol.* **186**, 693-702.

Stankunas, K., Hang, C. T., Tsun, Z. Y., Chen, H., Lee, N. V., Wu, J. I., Shang, C., Bayle, J. H., Shou, W., Iruela-Arispe, M. L. et al. (2008). Endocardial Brg1 represses ADAMTS1 to maintain the microenvironment for myocardial morphogenesis. *Dev. Cell* **14**, 298-311.

Staudt, D. and Stainier, D. (2012). Uncovering the molecular and cellular mechanisms of heart development using the zebrafish. *Annu. Rev. Genet.* **46**, 397-418.

Subach, O. M., Gundorov, I. S., Yoshimura, M., Subach, F. V., Zhang, J., Grüenwald, D., Souslova, E. A., Chudakov, D. M. and Verkhusha, V. V. (2008). Conversion of red fluorescent protein into a bright blue probe. *Chem. Biol.* **15**, 1116-1124.

Suri, C., Jones, P. F., Patan, S., Bartunkova, S., Maisonpierre, P. C., Davis, S., Sato, T. N. and Yancopoulos, G. D. (1996). Requisite role of angiopoietin-1, a ligand for the TIE2 receptor, during embryonic angiogenesis. *Cell* **87**, 1171-1180.

Tidcombe, H., Jackson-Fisher, A., Mathers, K., Stern, D. F., Gassmann, M. and Golding, J. P. (2003). Neural and mammary gland defects in ErbB4 knockout mice genetically rescued from embryonic lethality. *Proc. Natl. Acad. Sci. USA* **100**, 8281-8286.

Toyofuku, T., Zhang, H., Kumanogoh, A., Takegahara, N., Suto, F., Kamei, J., Aoki, K., Yabuki, M., Hori, M., Fujisawa, H. et al. (2004a). Dual roles of Sema6D in cardiac morphogenesis through region-specific association of its receptor, Plexin-A1, with off-track and vascular endothelial growth factor receptor type 2. *Genes Dev.* **18**, 435-447.

Toyofuku, T., Zhang, H., Kumanogoh, A., Takegahara, N., Yabuki, M., Harada, K., Hori, M. and Kikutani, H. (2004b). Guidance of myocardial patterning in cardiac development by Sema6D reverse signalling. *Nat. Cell Biol.* **6**, 1204-1211.

Trinh, L. A. and Stainier, D. Y. R. (2004). Fibronectin regulates epithelial organization during myocardial migration in zebrafish. *Dev. Cell* **6**, 371-382.

Trinh, L. A., Yelon, D. and Stainier, D. Y. R. (2005). Hand2 regulates epithelial formation during myocardial differentiation. *Curr. Biol.* **15**, 441-446.

Vermot, J., Forouhar, A. S., Liebling, M., Wu, D., Plummer, D., Gharib, M. and Fraser, S. E. (2009). Reversing blood flows act through klf2a to ensure normal valvulogenesis in the developing heart. *PLoS Biol.* **7**, e1000246.

Westerfield, M. (2000). *The Zebrafish Book: A Guide for the Laboratory Use of Zebrafish (Danio rerio)*. Eugene, OR: University of Oregon Press.